Article

Characterization of Electroless Nickel–Boron Deposit from Optimized Stabilizer-Free Bath

Muslum Yunacti [1,*], Alexandre Mégret [1], Mariana Henriette Staia [2], Alex Montagne [2] and Véronique Vitry [1]

1 Metallurgy Department, UMONS, 20 Place du Parc, 7000 Mons, Belgium; alexandre.megret@umons.ac.be (A.M.); veronique.vitry@umons.ac.be (V.V.)
2 Arts et Métiers Institute of Technology, MSMP, HESAM Université, F-59000 Lille, France; mhstaia@gmail.com (M.H.S.); alex.montagne@ensam.eu (A.M.)
* Correspondence: muslum.yunacti@umons.ac.be; Tel.: +32-4-6705-7882

Abstract: Conventional electroless nickel–boron deposits are produced using solutions that contain lead or thallium, which must be eliminated due to their toxicity. In this research, electroless nickel–boron deposits were produced in a stabilizer-free bath that does not include any toxic heavy metal. During processing, the plating rate increased from 10 to 14.5 μm/h by decreasing the concentration of the reducing agent, leading to increased bath stability. The thickness, composition, roughness, morphology, hardness, wear, and corrosion resistance of the deposits were characterized. The new deposit presents an excellent hardness of 933 ± 56 hv$_{50}$, 866 ± 30 hk$_{50}$, and 12 GPa from the instrumented indentation test (IIT), respectively, which are similar to that of hexavalent hard chromium coating. Moreover, by using both potentiodynamic polarization and salt spray tests it was shown that the coating presents higher corrosion resistance as compared to standard nickel-boron coatings. The new deposit exhibits properties close to those of the conventional electroless nickel–boron deposits. Therefore, it could replace them in any industrial applications.

Keywords: electroless nickel–boron deposit; environmentally friendly deposition; stabilizer; reducing agent; plating rate; characterization

1. Introduction

Electroless plating is a metal deposition from an aqueous solution. It is a chemical reduction process, which depends upon the catalytic reduction of metal ions in an aqueous solution. In this process, that uses no external current source, the electrons used to discharge metal ions are produced by the oxidation of the reducing agent [1–7].

Several coatings can be obtained from electroless deposition, but the most popular one is electroless nickel (EN) since it has a great ability to provide uniform, hard, wear-resistant, and corrosion-resistant coatings [1,5,6]. Therefore, many applications of EN coatings can be seen in several industries: aerospace, automotive, oil, electronics, mining, etc. [1,8–10]. One of the EN-coating classifications is based on the reduction agent. Electroless nickel–phosphorus coating (ENP) is obtained when hypophosphite is used. Meanwhile, electroless nickel–boron coating for its production employs borohydride or amine borane and pure nickel coating hydrazine, respectively [1,2,4]. However, deposits reduced by borohydride and hypophosphite are used more extensively than the others [11]. Among them, electroless nickel–boron from a borohydride reducing agent is the hardest and the most wear-resistant coating [1–4,12,13]. Therefore, this deposit attracts the interests of researchers and engineers as a prominent candidate to replace the hexavalent chromium coatings.

Apart from the nickel ion source and borohydride, numerous other components can be used in the electroless nickel–boron deposit bath, such as a stabilizer, complexing agent, buffering agent, surfactant, etc. Each component has a particular function during deposition [1–3,10]. Using a stabilizer, while its amount is a trace, has significant importance for conducting the process without a plate-out or a decomposition of the bath [4,14]. For

this purpose, many compounds, mainly heavy metals, have been used as stabilizers for the electroless nickel–boron deposit process. Lead and thallium have primarily been used as standard stabilizers for 30 years in the industry of electroless nickel–boron deposit [15]. However, the emergence of new legislation dictates the limitation in using Pb [16] and Tl in the EN deposition baths [17].

Today, the lead content in the coating and the deposition bath used in industry is within the limits of the legislation [17,18]. On the other hand, as the legislation regarding environmental subjects is regularly strengthening, increased demand for completely removing lead and thallium from EN deposition baths has been seen in the metal deposition market. In addition, a few completely lead and thallium-free baths have been presented for electroless nickel–boron deposition [15,17,19,20]. One of them, developed by Bonin et al. [17], completely removed the stabilizer agent from the bath and stabilized the bath by optimizing complexing agent concentration.

Besides the stabilizer and the complexing agent, many parameters, such as reducing agent concentration, pH, and temperature of the deposition bath, can significantly impact the bath stability and plating rate [2,4,21]. All the other parameters in the bath formulation have already been optimized except the reducing agent and nickel source; however, the former one is more impactful on the bath stability and coating properties [10].

The decomposition of the deposition bath has been attributed to reducing excess Ni^{2+} to the metallic state in the bulk of the solution [22,23]. An increase in the $NaBH_4$ concentration can result in many electrons, which are used to reduce Ni^{2+} ions. The correlation between the bath stability and Ni^{2+} ions reduction is inversely proportional: a decrease in $NaBH_4$ can increase the bath stability [4], as documented by Mallory G.O. in a stabilizer-free bath [24]. However, it is noteworthy to mention that an important decrease in the $NaBH_4$ concentration may result in a low plating rate since the oxidation of $NaBH_4$ is the rate-determining step [2,10,14,24]. Therefore, the $NaBH_4$ concentration must be chosen precisely to obtain a thick deposit and a well-stabilized bath.

The purpose of the present research work is to improve the composition of the stabilizer-free bath developed by previously by Bonin et al. [17]. In their research, the plating rate is about 10 μm/h, hardness and wear resistance are lower than that of the conventional electroless nickel–boron stabilized by lead, but the corrosion resistance is better than the conventional one. For this purpose, several baths that contain different $NaBH_4$ concentrations were prepared to determine the most suitable bath composition using the surface roughness of the deposit and the plating rate as selection criteria. These two parameters are good indicators of several characteristics of the process. The surface roughness provides information about the bath stability, and the plating rate was evaluated to ensure sufficient productivity. After the change in $NaBH_4$ concentration, the surface morphology, composition, mechanical, tribological, and corrosion properties were analyzed.

2. Materials and Methods

2.1. Substrate Preparation

ST 37-DIN 17100 mild steel with dimensions of $50 \times 25 \times 1$ mm^3 was used as the substrate in these experiments. Substrate grinding was carried out with SiC paper of 180, 500, and 1200 grit.

Subsequently, the substrates were cleaned in acetone before activation. Activation was carried out in 30 vol.% HCl acid for 3 min. Rinsing with distilled water was done after each step. After the activation step, the samples were immediately immersed in the deposition bath for one hour.

2.2. Electroless Nickel Baths

The electroless nickel–boron deposition baths are shown in Table 1. The deposition baths (1 L) were prepared on a regulated hot plate with magnetic stirring. The temperature was fixed at 95 ± 1 °C during the deposit process for all samples. As a comparison, electroless nickel–boron deposits from the lead stabilized bath (ENB-Pb), which was de-

veloped by Delaunois et al. [25] (see composition in Table 1), were prepared following the same procedure.

Table 1. The composition of stabilizer-free bath and lead-stabilized bath.

Compound	Stabilizer-Free Bath	Lead-Stabilized Bath [25]
$NiCl_2 \cdot 6H_2O$ (g/L) (99%—VWR Chemicals, Radnor, PA, USA)	24	24
$NaBH_4$ (g/L) (99.9%—Acros Organics, Fair Lawn, NJ, USA)	Variable	0.602
$NH_2\text{-}CH_2\text{-}CH_2\text{-}NH_2$ (mL/L) (99% VWR Chemicals, Radnor, PA, USA)	120	59
NaOH (g/L) (VWR Chemicals, Radnor, PA, USA)	160	39
$PbWO_4$ (g/L) (MaTeck GmbH, Jülich, Germany)	-	0.021

In this study, seven different baths with different $NaBH_4$ concentrations (0.6, 0.55, 0.5, 0.45, 0.4, 0.35 and 0.3 g/L, respectively), were prepared. Three samples were produced in each set of conditions.

2.3. Characterization

A HIROX KH-8700 (Tokyo, Japan) digital optical microscope was used to determine the plating rate. The plating thickness was measured in the cross-section of the samples prepared by setting them in a resin polishing using standard metallographic procedure up to mirror finish and, subsequently, etching with Nital 10% for 2 min.

A Zeiss 119 Surfcom 1400D-3DF (Oberkochen, Germany) apparatus was employed to measure deposit surface roughness, and Zeiss brand software is used for analyzing the results. Three different roughness values, namely average (R_a), peak (R_p), and valley (R_v) roughness, were determined. The values are the average of ten measurements per sample.

A Hitachi SU8020 (Tokyo, Japan) scanning electron microscopy (SEM) was used to analyze the surface and the cross-section morphology of each sample.

The composition of the coatings was determined by glow discharge optical emission spectroscopy (GDOES) using a Horiba Scientific GD Profiler 2 (Kyoto, Japan).

The hardness of samples was measured by Knoop microindentation on the cross-section, with a load of 50 gf and a holding time of 20 s. However, Vickers microindentation was performed on the top surface, using a load of 50 gf and the same holding time. A Mitutoyo HM-200 (Kawasaki, Japan) microhardness tester was employed to determine the hardness of the deposits. The reported values are the average of ten measurements.

Additionally, to determine the elastic properties of the deposits, the indentation tests were carried out on the sample cross-section using a nanoindenter XP (MTS, Eden Prairie, MN, USA) equipped with a Berkovich indenter in continuous stiffness measurement (CSM) mode with an imposed maximum penetration depth of 300 nm. The tip was calibrated using fused silica. The load–displacement curves were analyzed by the method of Oliver and Pharr [26]. To perform the test, coatings were set in a cold resin (DuroFast, Struers, Copenhagen, Denmark), then mechanically polished with SiC paper (from grit 80 to grit 4000), followed by polishing with diamond paste (1 and 3 μm), then with a colloidal silica suspension.

A Tribotechnic (Clichy, France) scratch tester machine with a diamond Rockwell stylus with a radius of 200 μm was employed to carry out scratch tests. In all cases, a linearly increasing load from 0 to 150 N was used with a scratch velocity of 6.75 mm/min. The scratch length was set to be 10 mm. Acoustic emission and friction coefficient were monitored during the experiments. Hitachi SU8020 SEM and A HIROX KH-8700 digital optical microscope were used to analyze the deposit adhesion on the scratched substrate.

A ball-on-disc Tribotechnic microtribometer without lubrication was employed to investigate the tribological behavior of the deposit. The samples served as the disc and alumina balls with 6 mm diameter used as counterpart. The sliding speed and normal

loads were 0.1 m/s and 5 N, respectively. The sliding distance was 1000 m; the wear track diameter was 6 mm. Wear tests were carried out in the ambient environment. During the tests, the friction coefficient was continuously recorded. The digital optical microscopy HIROX KH-8700 and Hitachi SU8020 SEM were used for the surface analyses after the ball-on-disc. Energy-dispersive X-ray spectroscopy (EDX)–Hitachi SU8020 SEM was employed to determine the surface composition of the wear track after the ball-on-disc test.

A Bio-Logic (Claix, France) SP-300 potentiostat was used to obtain potentiodynamic polarization curves in 0.1 M NaCl solution. A standard three-electrode cell was used to carry out the tests. The sample was the working electrode, the platinum plate was the counter electrode, and Ag/AgCl (KCl saturated) was the reference electrode. The potential range and scan rates were ±0.25 V vs. OCP and 1 mV/s, respectively.

Neutral salt spray tests were carried out in a Q-FOG cyclic corrosion tester (Q-Lab, Westlake, OH, USA), according to ASTM B117-07. The surface exposed to salt spray was the same for all samples. The surface exposed to the saltwater was a sphere with a 0.6 mm radius. The samples were suspended in the cabinet for 10 days with a period of 1 h, 4 h, 8 h, 1, 2, 3, 4, 5, 7 days control, and image taking. ImageJ, an open-source image processing analysis program, was used to quantify the corroded area after the salt spray test.

3. Results and Discussion

3.1. The Impact of $NaBH_4$ Concentration on Plating Rate and Roughness

The thickness and roughness obtained from baths with varying $NaBH_4$ concentrations are shown in Figure 1. The most promising bath was the one containing 0.4 g/L $NaBH_4$. This result is coherent with the literature. Without a stabilizer, the plating rate increased with $NaBH_4$ content at low concentrations, but when a threshold was passed, further increase led to the destabilization of the plating solution and thus to lower plating rated [10]. The impact of the $NaBH_4$ concentration on the deposit roughness was negligible, as shown in Figure 1.
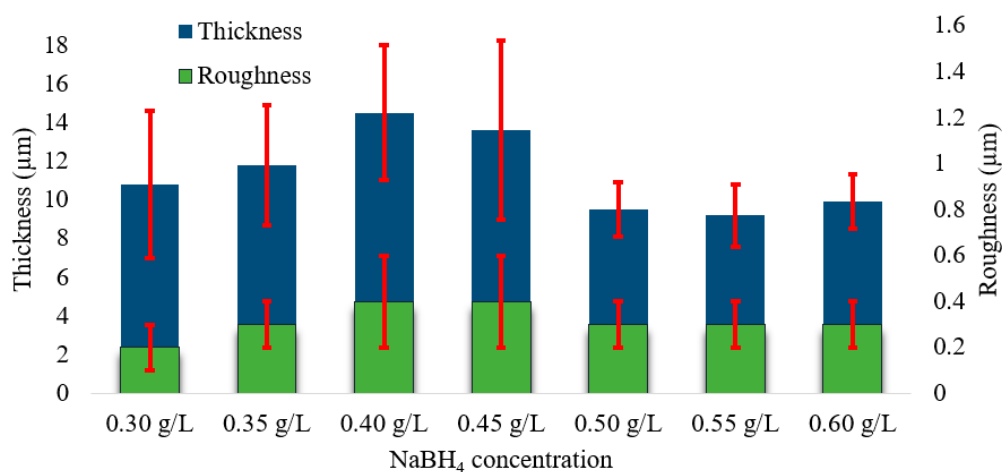

Figure 1. Thickness and roughness of the deposits from a different set of conditions.

The coating produced in the optimized EN bath, which contains 0.4 g/L $NaBH_4$ of reducing agent, was investigated in terms of morphology, chemical profile, hardness, tribological, and corrosion resistance. Hereafter, the deposit produced using the optimized EN bath without stabilizer will be referred to as ENB and will be compared to the ENB-Pb deposit.

3.2. Morphology of the ENB Coatings

The morphological properties of both ENB coatings and ENB-Pb one are presented in Figure 2. The ENB-Pb surface morphology presents the typical cauliflower-like morphology, and its cross-section morphology is as expected columnar [27–29]. However, the new

deposit from the stabilizer-free bath exhibited neither the typical cauliflower-like structure nor the columnar morphology in its cross-section. Its surface was uniform and smooth-looking, and its cross-section featureless and dense even after Nital etching. It is known that the cauliflower-like morphology and columnar features of electroless nickel–boron deposits are linked to the presence of heavy metal stabilizers that limit the lateral growth of the coating [17,30]. It was thus expected that their absence would modify the growth of coatings. An in-depth study of the growth of this newly developed system will be the object of further work.


(a)

(b)

(c)

(d)
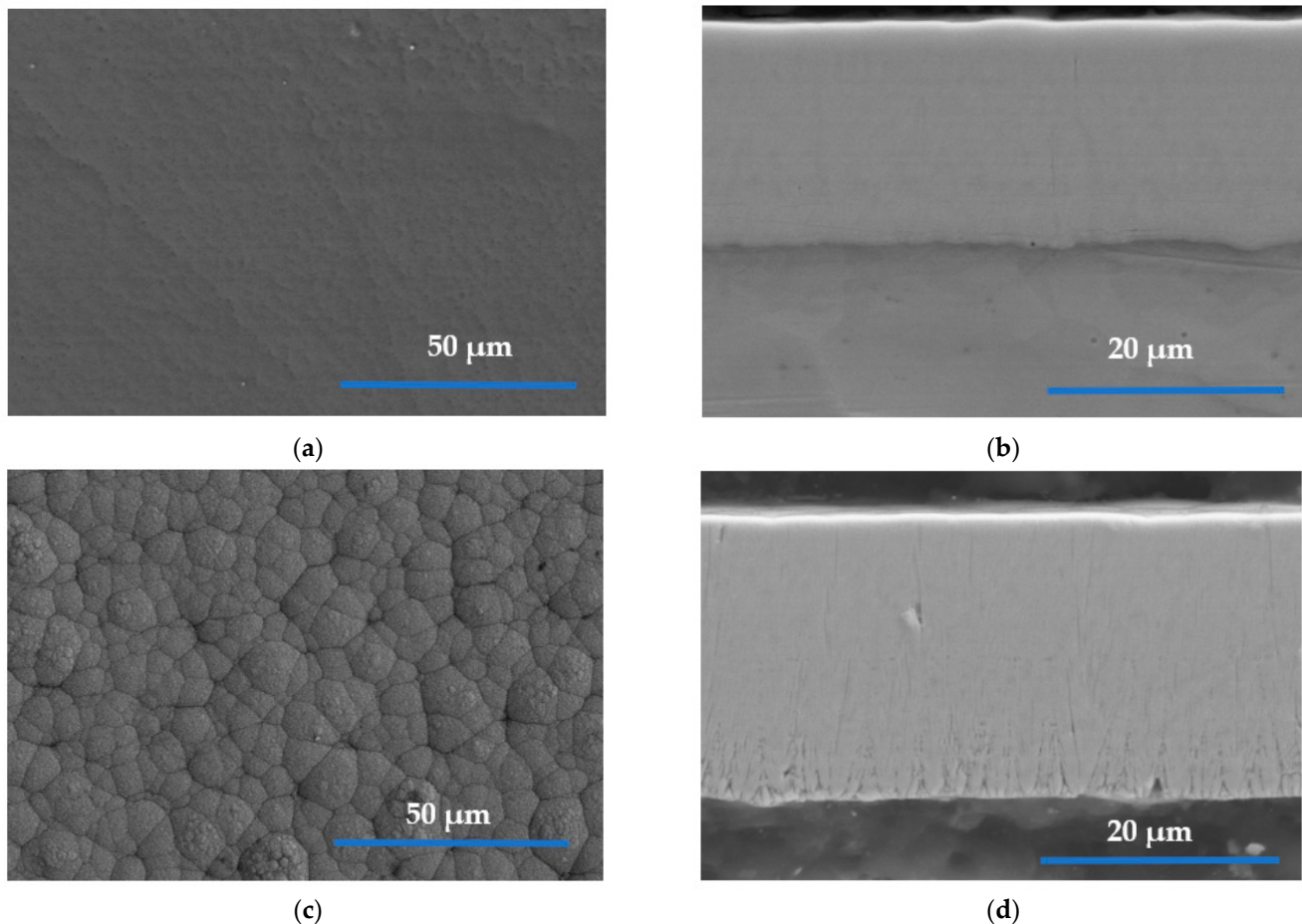
Figure 2. SEM micrograph of the ENB and ENB-Pb deposits: (**a**) surface morphology of ENB, (**b**) cross-section morphology of ENB, (**c**) surface morphology of ENB-Pb, and (**d**) cross-section morphology of ENB-Pb.

Comparing this work with a previous study on stabilizer-free, it seemed there is no effect of the $NaBH_4$ concentration on the morphology of the deposit: the present deposit, obtained with 0.4 g/L $NaBH_4$ and the one from Bonin et al. (that had 0.602 g/L $NaBH_4$) [17], display the same surface and cross-section morphology.

3.3. Profile Chemistry

The results of the GDOES analysis are presented in Figure 3 and Table 2. The average boron content in the deposits from the stabilizer-free bath was 4 wt.%. The rest was nickel. The boron content was significantly lower than in the previous study [17] due to a decrease of the reducing agent, which is the only boron source compound in the bath, concentration from 0.602 to 0.4 g/L. The boron content in the lead-stabilized bath was 5.5 wt.% and around 1 wt.% lead. It was determined that there was no significant variation in the boron content throughout the coating thickness, either for the coating ENB or ENB-Pb. However, a slight decrease in the boron content was observed from the substrate to the surface due

to the quick consumption of the reducing agent at the beginning of the process. Vitry [2] showed that more borohydride is used at the beginning of the process.

(a)

(b)
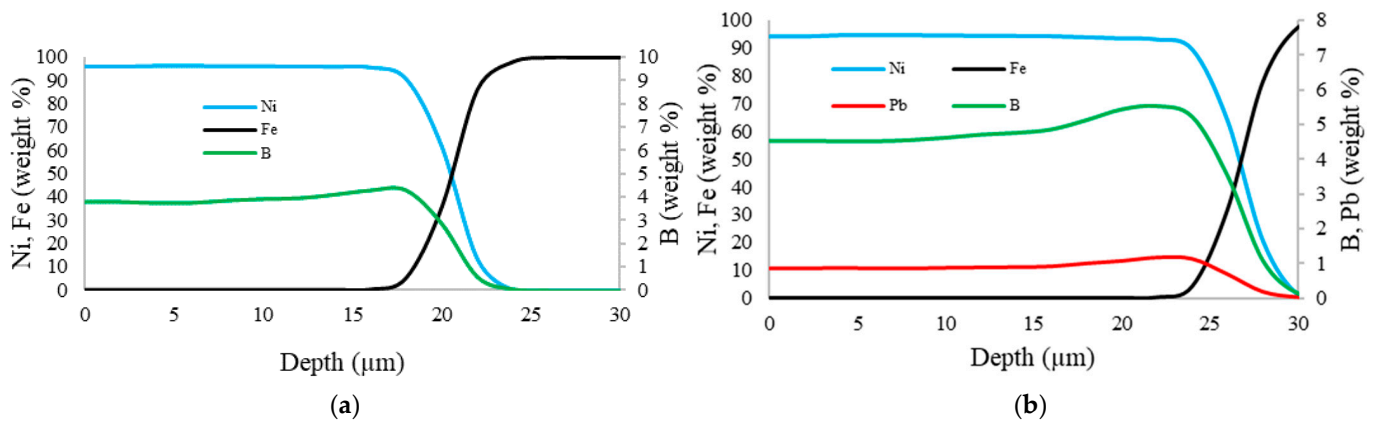
Figure 3. Depth profile chemical analysis of the EN deposits: (**a**) ENB and (**b**) ENB-Pb.

Table 2. Chemical composition of the coating from GDOES experiments.

Element	ENB	ENB-P
Ni (wt.%)	96.0 ± 0.3	93.5 ± 0.3
B (wt.%)	4.0 ± 0.1	5.5 ± 0.2
Pb (wt.%)	-	1.0 ± 0.1

3.4. Roughness

The results of roughness measurements are shown in Table 3. The roughness of the substrates was maintained after the EN deposit since it grew uniformly on the substrates and thus did not modify the morphology of the substrates [31]. The both deposits present similar roughness. Moreover, the peak roughness of the ENB deposit was higher than that of the ENB-Pb deposit, which might be attributed to the superior stability of the ENB-Pb bath. Higher bath stability could block precipitate formation, which could adhere to the deposit during the process. However, in the case of the ENB deposit, a slight amount of precipitate was formed.

**Table 3.** Roughness, ball-on-disc and scratch test results.

Measurements	ENB	ENB-Pb
Average roughness (μm)	0.3 ± 0.1	0.3 ± 0.1
Peak roughness (μm)	1.9 ± 1.2	1.2 ± 0.3
Valley roughness (μm)	1.3 ± 0.4	1.5 ± 0.5
Wear track (μm)	368 ± 17	335 ± 24
Friction coefficient (μ)	0.47	0.51
Critical load Lc (N)	22.7 ± 4.3	24.7 ± 5.4

3.5. Hardness

The hardness results are presented in Table 4. The hardness of the ENB deposits was similar to that of ENB-Pb deposits both on surface and cross-section. Moreover, the same outcome was also encountered in the results of the nanoindentation. Depth profile evolution of hardness and Young's modulus are shown in Figure 4 and in Table 4, respectively, and it was clear that the hardness of these two deposits was homogeneous throughout the coating thickness.

Table 4. Hardness and elastic modulus results.

| Measurements	ENB	ENB-Pb
Vickers hardness (hv$_{50}$)	933 ± 62	896 ± 57
Knoop hardness (hk$_{50}$)	886 ± 30	892 ± 87
Hardness IIT (GPa)	11.6 ± 0.3	11.5 ± 0.7
Elastic modulus (GPa)	201 ± 10	185 ± 10
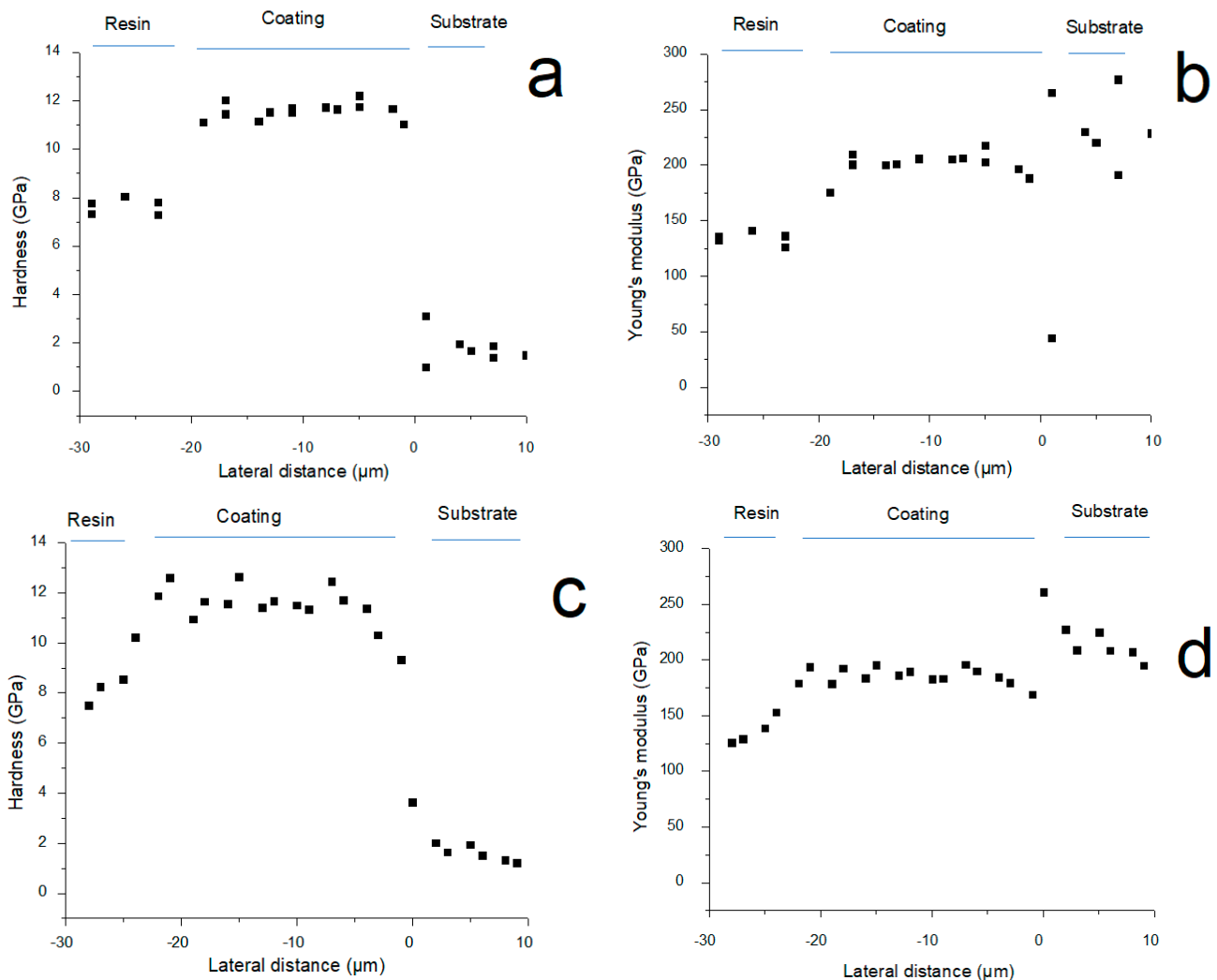
Figure 4. Hardness (**a**) and Young's modulus (**b**) of the ENB deposit, hardness (**c**), and modulus (**d**) of the ENB-Pb deposit.

It is interesting to note that the coatings had similar hardness even if they had different boron content. The correlation between hardness and the boron content has not been well revealed. Some authors have shown an increase of hardness with the boron content of nickel–boron deposits [17]. However, these results cannot be directly compared to the findings of the present work since the process was carried out by codeposition of heavy metal (thallium), whose effect has not been fully elucidated. On the other hand, Vitry and Bonin [32] reported similar values as our research for the hardness of the deposits containing 8 wt.% to 6 wt.% B. Moreover, the compilation [3] of the results of different research groups related to the hardness values of electroless nickel–boron deposits has been shown that these were independent of the boron content. In addition to these, Lee et al. [33] studied electrodeposited nanocrystalline Ni-B alloy films, and they reported that deposits containing 4 wt.% B and 6 wt.% B exhibited the same hardness. Despite the different

fabrication methods, their composition closer to ours than typical electroless nickel–boron due to the absence of co-deposited heavy metal. The similar hardness values for ENB and ENB-Pb were not in line with Bonin's observation that the third element in the deposit could favorably modify hardness. Further microstructural characterization of the stabilizer-free coatings will be carried out in the future to elucidate this phenomenon.

3.6. Scratch Test

Table 3 presents the critical load (Lc) of the deposit from the different baths. The Lc refers to the first damage presented by the coatings under load. It was determined by a combination of acoustic emission and microscopical observation. Despite their differences in thickness, the first damage observed indicated chevron cracks appearing at 22.7 ± 4.3 N and 24.7 ± 5.4 N for the ENB deposits and ENB-Pb deposits, respectively. Figure 5 shows the scratched surface of the deposits at the beginning of the scratch.

(**a**)	(**b**)
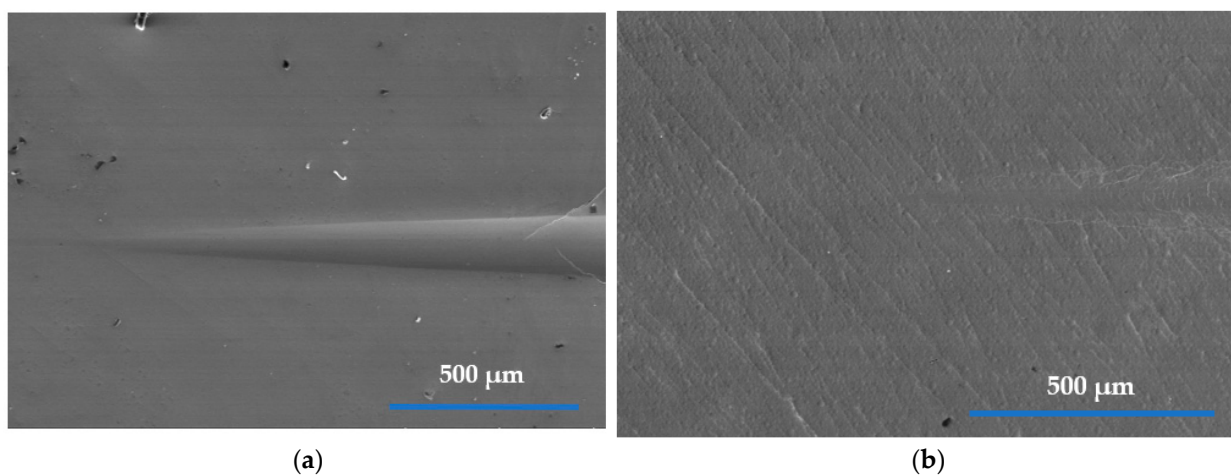
Figure 5. SEM images appearing at the beginning of the scratch test: (**a**) the ENB deposit, (**b**) the ENB-Pb deposit.
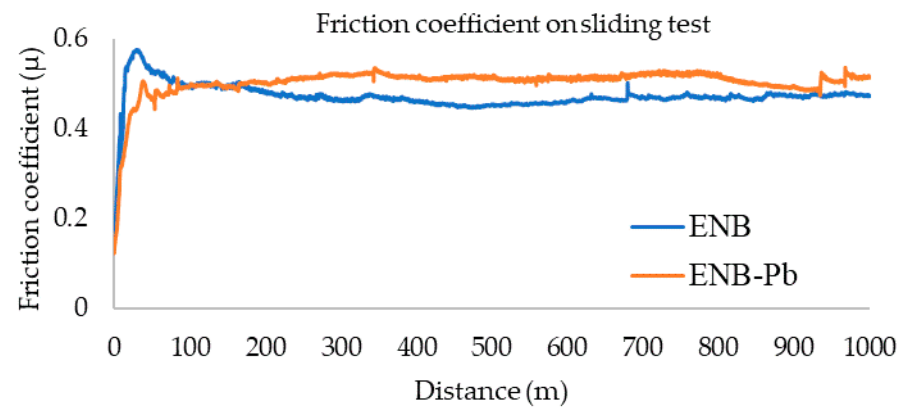
3.7. Ball-on-Disc Wear Test

The wear data obtained for the two deposits using ball-on-disc apparatus in non-lubricated conditions are given in Figures 6–9 and Tables 3, 5 and 6. Figure 6 presents the friction coefficient (COF) of the deposits. There is no significant fluctuation in the COF of the deposits, but there is more variation in the ENB-Pb deposit compared to ENB. This might be attributed to a variation in the surface morphology: the ENB-Pb deposit presented the typical cauliflower-like structure, which led to variations in the contact area throughout the test. At the beginning, the increase in the COF was similar to that reported by several researchers [19,34–37]. Also, it was observed that the ENB deposit's COF stabilized sooner than one of the ENB-Pb deposits, probably due to its smooth surface morphology [17].

The ENB deposit's wear track width was higher than that of the ENB-Pb deposit, as shown in Table 3. ENB-Pb thus presented better wear resistance, even though ENB had a lower COF, which follows several studies [11,38]. However, Correa observed a different behavior with a wear rate directly proportional to COF [39].

Additionally, the worn surfaces and their composition after the ball-on-disc test were analyzed by SEM, as shown in Figure 7 and Table 5, respectively. The chemical analysis was done on the regions, which are indicated as 1, 2, or 3 in the SEM micrographs. The SEM micrographs of the ENB-Pb deposit after the ball-on-disc wear test explicitly indicated that no formation of debris after the 1000 m ball-on-disc test occurred, unlike the ENB deposit, which has a considerable amount of debris after the test. This observation also shows that, apparently, the ENB-Pb deposit has a better wear resistance than the ENB deposit. However, as shown below, this result is mainly a consequence of both the relatively small thickness of the ENB deposit and the lack of the load support of the steel substrate.

Figure 6. Friction coefficient variation with the sliding distance for the ENB deposit and the ENB-Pb deposit.
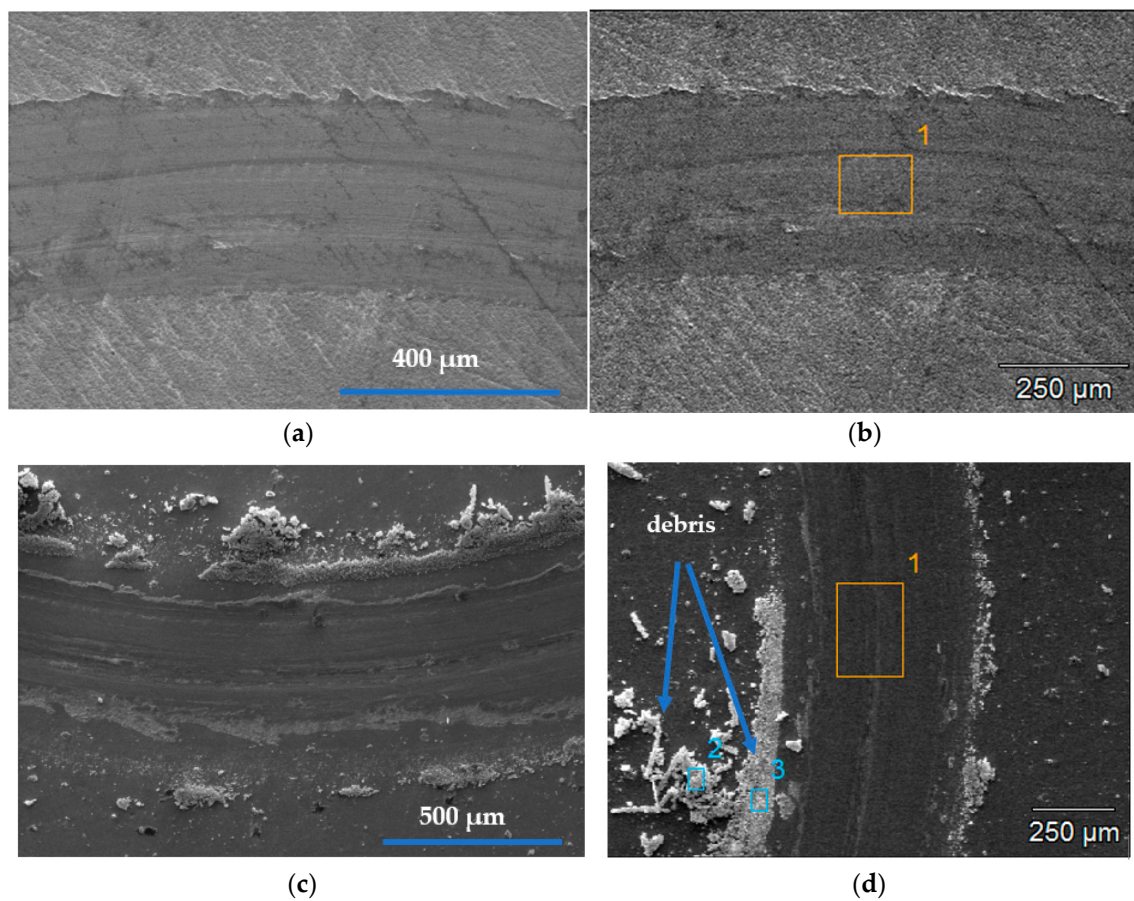
Figure 7. SEM micrographs of ball-on-disc wear tracks: (**a**,**b**) from the ENB-Pb deposit, (**c**,**d**) from the ENB deposit.
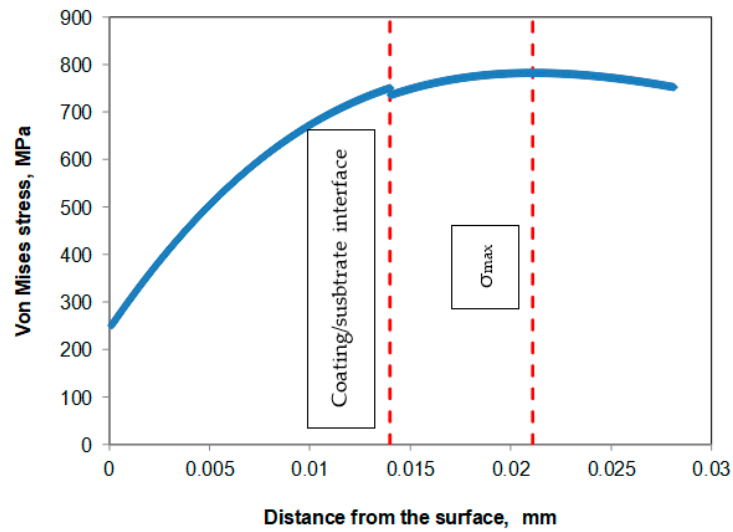
Figure 8. Variation of the von Mises stress with distance from the ENB deposit surface under 5 N load.
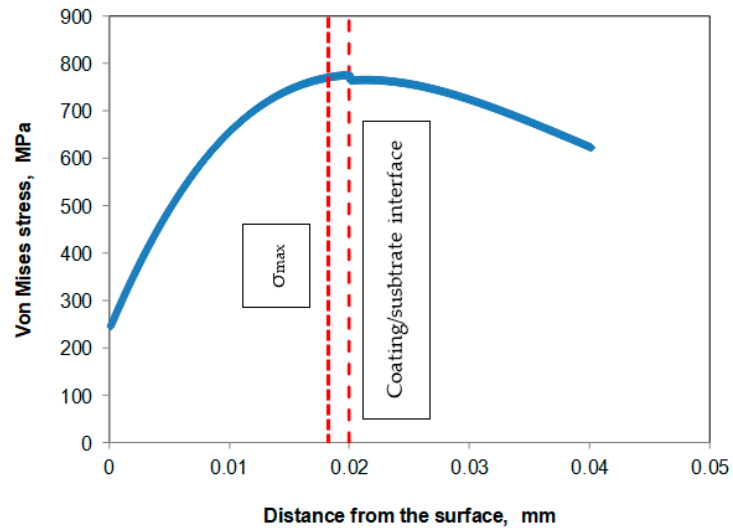

Figure 9. Variation of the von Mises stress with distance from the ENB-Pb deposit surface under 5 N load.

Table 5. Chemical composition of the wear track on the deposits and debris by EDX.

Element	Carbon (C) (wt.%)	Oxygen (O) (wt.%)	Aluminum (Al) (wt.%)	Iron (Fe) (wt.%)	Nickel (Ni) (wt.%)
ENB-Pb	1.6 ± 0.3	11.3 ± 1.6	1.0 ± 0.1	-	86.1 ± 1.8
ENB	1.4 ± 0.1	11.6 ± 1.0	1.0 ± 0.1	0.4 ± 0.2	85.6 ± 0.8
Debris	2.3 ± 0.3	28.2 ± 2.3	2.5 ± 0.3	0.2 ± 0.2	66.6 ± 2.4

Table 6. Data needed to calculate the P_{max} using Hertz formulation.

Properties / Material	E (GPa)	Thickness (μm)	Poisson's Ratio (v)	P_{max} (GPa)	Von Mises Max Stress σ_{max} (MPa)	Yield Stress σ (MPa)
ENB	201	14	0.31	1.29	784	3870
ENB-Pb	185	20	0.31	1.26	776	3830
Steel	210	-	0.33	-	-	400
Al_2O_3	360	-	0.2	-	-	-

Thus, as shown in Figure 7, in the case of the ENB-Pb deposit, the typical cauliflower-like structure was completely worn away in the track zone, and the worn surface appears to be smooth, which also has been reported by Bonin et al. [38] and Mukhopadhyay et al. [11]. However, in the case of the ENB deposit, deep grooves were present in the middle of the wear track zone, which could be due to the plowing action of the strain hardened debris, indicating an abrasive wear mechanism.

Table 5 presents the composition analysis of the deposit and debris. The composition in the wear track was similar for both deposits, but a slight amount of iron was observed in the wear track in the ENB deposit, indicating that the coating had fractured and delaminated. An important amount of oxygen indicated oxidation due to elevation of temperature by friction between the ball and the deposits. Debris composition was noticeably different from that in the wear track. More oxygen and less nickel were observed in the debris than the amount found in the latter.

The behavior of the investigated electroless deposits could be explained as follows: by knowing the elastic properties of both deposits, the Al_2O_3 ball and steel substrate, the maximum contact pressure (P_{max}) and maximum von Mises stress (σ_{max}) can be computed using the Hertz formulation [40] and data given in Table 6. Accordingly, it was determined that for the ENB-Pb deposit, P_{max} = 1.2 GPa, whereas for the ENB deposit P_{max} = 1.29 GPa.

In Table 6, the yield stress of the deposits is assumed to be one-third of the hardness determined by nanoindentation measurements [41]. Thus, it can be clearly observed that the contact pressures calculated in the conditions of the wear tests are much higher than the typical maximum contact pressures that are found in the industrial applications of these coatings. In the ENB deposit, with a thickness of 14.5 μm, σ_{max} = 784 MPa and it is predicted to occur at a depth of approximately 21 μm from the coating surface. Therefore, it is expected that the substrate will be deformed plastically since it is much higher than the yield stress of the steel substrate (see Figure 8). This computation allows the understanding of the wear results presented above. The plastic deformation of the substrate implies that the coating will not have the appropriate load support from the substrate and, therefore, it will fracture and delaminate more easily, corroborating the SEM observations shown in Figure 7. Consequently, the wear behavior observed for the ENB deposit is not determined by its microstructure and mechanical properties but mainly by its thickness and the lack of load support from the steel substrate.

On the other hand, in ENB-Pb, with a thickness of 20 μm, σ_{max} = 776 MPa and it was found to be located close to the substrate-coating interface, inside the electroless deposit, whose yield stress was much higher than σ_{max}. This observation explains the better wear performance of this coating (as shown in Figure 9), which was mainly due to its higher thickness.

Hertz formulation also allows the prediction that the maximum von Mises stress in an ENB deposit of 14.5 μm in thickness would be located inside the coating and close to the interface if the load applied during the wear test was of 2 N, at the most, ensuring a maximum contact pressure of approximately P_{max} = 0.95 GPa., which is quite acceptable in any practical application of this coating. Therefore, it can be concluded that the difference in wear behavior exhibited by both coatings was rather a consequence of the difference in thickness and lack of support of the steel substrate than a difference in the microstructure and mechanical properties of the coatings.

3.8. Corrosion Tests

Figure 10 shows the potentiodynamic polarization tests for the substrate, the ENB deposit, and the ENB-Pb deposit. Both deposits shifted the corrosion potential positively compared to the substrate, which was expected as electroless nickel deposits are used as a barrier coating, and the corrosion potential of nickel was much higher than that of iron [17]. Moreover, the E_{corr} of the ENB deposit was more positive than the one of the ENB-Pb deposit.
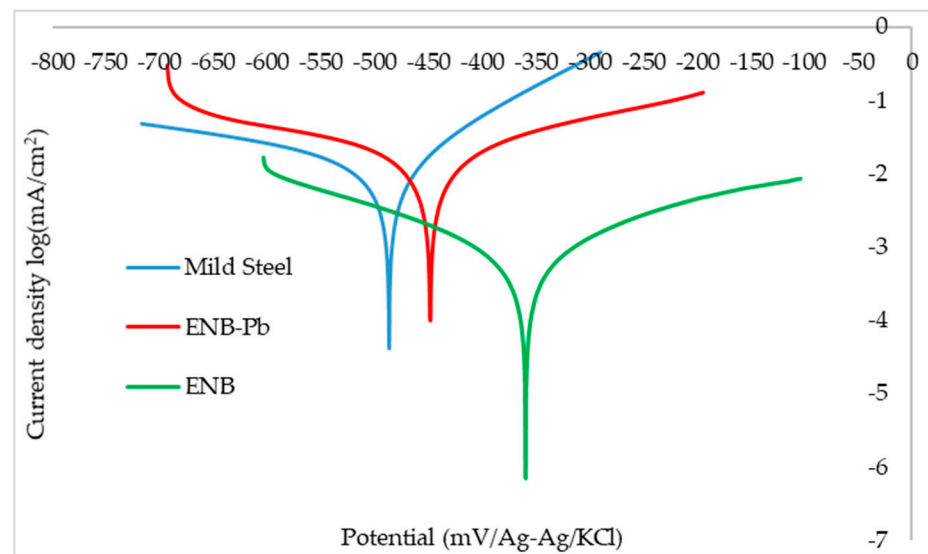
Figure 10. Potentiodynamic polarization curves of mild steel, the ENB deposit, and the ENB-Pb deposit.

The results of the salt spray test, which are depicted in Figure 11, were coherent with the potentiodynamic polarization resulted. In the neutral salt spray test, mild steel started to corrode after one hour, while the coated samples started to corrode later: after 48 h for the ENB deposit and after 24 h for the ENB-Pb deposit. Mild steel was completely corroded after 1 day in the salt spray test. On the other hand, after 7 days, only 3.5% of the ENB coating was corroded, and only 11% of the ENB-Pb coating. The corroded area of the ENB coating was only 7.2%, much lesser than the 17% measured on the ENB-Pb coating after 10 days of neutral salt spray. In all cases, it was noticed that corrosion started at the edge of the samples, which could be resulted from saltwater entrapment between the edge of the samples and the masking tape. Baskaran et al. [42] highlighted that there were several factors, such as coating thickness, porosity, deposit chemistry, structure, heterogeneity in deposits, and surface and cross-sectional morphology of the deposits, which could highly affect the corrosion properties of the coating. The better behavior of the ENB coating could be due to the absence of lead, which could make the coating less heterogeneous than the ENB-Pb one. The improved smoothness of the ENB coating compared to the ENB-Pb coating could also play a role: Kanta et al. [43] mentioned that the smoother surface favorably influenced the corrosion resistance of coatings. Moreover, both Bonin et al. [44] and Baskaran et al. [42] emphasized that the columnar structure had a detrimental effect on the electroless nickel coating since the intercolumnar zones could act as a penetration path for the corrosive medium. The absence of columnar structure could thus also play a positive role in the corrosion resistance response of ENB. In addition, it is noteworthy that the thickness of the ENB deposit was 14.5 μm, lower than that of the ENB-Pb deposit.
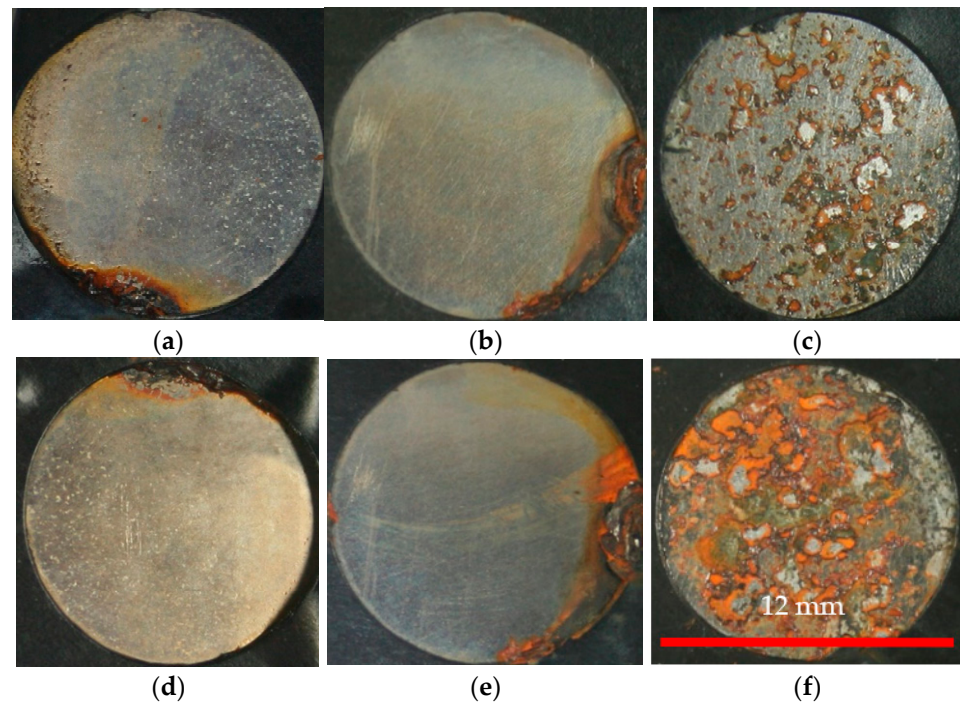
Figure 11. Surface appearance of ENB and ENB-Pb deposit, and mild steel during salt spray test: (**a**) seven days after the ENB deposit, (**d**) ten days after the ENB deposit, (**b**) seven days after the ENB-P deposit (**e**) ten days after the ENB-Pb deposit, (**c**) one hour after mild steel, and (**f**) one day after mild steel.

4. Conclusions

- The reducing agent content of an electroless nickel–boron plating bath exempt of stabilizer was optimized;
- The ENB deposit was produced in a bath exempt of lead whose application and use have been restricted. Therefore, this deposit can be used as an alternative to conventional electroless nickel plating for several practical applications;
- The productivity of the process in the new bath increased from 10 to 14.5 µm/h;
- The difference in wear behavior exhibited by both deposits was due to the variation in the coatings thickness and the lack of support of the steel substrate and not a consequence of their intrinsic properties;
- The ENB deposit presented a distinct morphology from usual electroless nickel–boron coatings: the new deposits do not present a cauliflower-like structure nor a columnar structure. On the contrary, their surface morphology was featureless and uniform;
- The chemical composition of the new coating was also significantly different from standard electroless nickel–boron. First, it did not contain lead, which is highly favorable from the environmental point of view. Second, the boron content was lower than in conventional nickel–boron or previously reported ENB deposits. The new deposits had approximately 4 wt.% B and 96 wt.% Ni;
- The new deposits present high hardness, which was close to or better than the conventional electroless nickel–boron deposit. This result was confirmed by three different tests: micro-Vickers, micro-Knoop, and nanoindentation;
- One of the most promising results was corrosion resistance, which improved due to the modification in the surface and cross-sectional morphology and the change in the chemical composition of the coating;

In future work, characterization of the newly developed coating system will be continued, mostly by carrying out their structural characterization, the study of initiation and growth of the coating in the absence of stabilizer, and the influence of the heat treatments that will allow optimizing their mechanical properties.

References

1. Riedel, W. *Electroless Nickel Plating*; Finishing Publications: London, UK, 1989; ISBN 0-904477-12-6.
2. Vitry, V. Electroless Nickel-Boron Deposits: Synthesis, Formation and Characterization; Effect of Heat Treatments; Analytical Modeling of the Structural State. Ph.D. Thesis, University of Mons, Mons, Belgium, 2009.
3. Delaunois, F.; Vitry, V.; Bonin, L. *Electroless Nickel Plating, Fundamentals to Applications*; Taylor&Francis Group: Abingdon-on-Thames, UK, 2019; ISBN 13:978-1-138-60580-0.
4. Bonin, L. Replacement of Lead Stabilizer in Electroless NiB Baths: New Composition of Green Baths with Properties Characterization. Ph.D. Thesis, University of Mons, Mons, Belgium, 2018.
5. Srinivasan, K.N.; Meenakshi, R.; Santhi, A.; Thangavelu, P.R.; John, S. Studies on development of electroless Ni-B bath for corrosion resistance and wear resistance applications. *Surf. Eng.* **2010**, *26*, 153–158. [CrossRef]
6. Venkatakrishnan, P.G.; Mohamed Nazirudeen, S.S.; Sankara Narayanan, T.S.N. Electroless Ni-B-P ternary alloy coatings: Preparation and evaluation of characteristic properties. *Eur. J. Sci. Res.* **2012**, *82*, 506–514.
7. Zhang, B. *Amorphous and Nano Alloys Electroless Depositions*; Elsevier: Changsha, China, 2016; ISBN 978-0-12-802685-4.
8. Taheri, R.; Oguocha, I.N.A.; Yannacopoulos, S. Effect of coating parameters and heat treatment on the adhesive properties of electroless Ni-P coatings. *Can. Metall. Q.* **2004**, *43*, 363–370. [CrossRef]
9. Anık, M.; Körpe, E.; Baksan, B. Isıl işlemin akımsız Ni.B kaplamanın mikro-yapısına, korozyond, rencine ve sertliğine etkisi. *J. Eng. Archit. Fac. Eskişehir Osmangazi Univ.* **2009**, *22*, 111–124.
10. Anik, M.; Körpe, E.; Şen, E. Effect of coating bath composition on the properties of electroless nickel-boron films. *Surf. Coat. Technol.* **2008**, *202*, 1718–1727. [CrossRef]
11. Mukhopadhyay, A.; Barman, T.K.; Sahoo, P.; Davim, J.P. Comparative study of tribological behavior of electroless Ni-B, Ni-B-Mo, and Ni-B-W coatings at room and high temperatures. *Lubricants* **2018**, *6*, 67. [CrossRef]
12. Pal, S.; Verma, N.; Jayaram, V.; Biswas, S.K.; Riddle, Y. Characterization of phase transformation behaviour and microstructural development of electroless Ni-B coating. *Mater. Sci. Eng. A* **2011**, *528*, 8269–8276. [CrossRef]
13. Matik, U. Improvement of surface properties of iron based powder metal compacts by electroless NiB coating. *J. Fac. Eng. Archit. Gazi Univ.* **2018**, *33*, 1603–1610. [CrossRef]
14. Cheong, W.J.; Luan, B.L.; Shoesmith, D.W. The effects of stabilizers on the bath stability of electroless Ni deposition and the deposit. *Appl. Surf. Sci.* **2004**, *229*, 282–300. [CrossRef]
15. Bonin, L.; Vitry, V.; Delaunois, F. The tin stabilization effect on the microstructure, corrosion and wear resistance of electroless NiB coatings. *Surf. Coat. Technol.* **2019**, *357*, 353–363. [CrossRef]
16. Williams, R.; Keeling, W.; Petsinaris, F.; Baron, Y.; Mehlhart, G. *Supporting the evaluation of the Directive 2000/53/EC on end-of-life vehicles*; Trinomics B.V.: Rotterdam, The Netherlands, 2020.
17. Bonin, L.; Castro, C.C.; Vitry, V.; Hantson, A.L.; Delaunois, F. Optimization of electroless NiB deposition without stabilizer, based on surface roughness and plating rate. *J. Alloys Compd.* **2018**, *767*, 276–284. [CrossRef]
18. Sahoo, P.; Das, S.K. Tribology of electroless nickel coatings—A review. *Mater. Des.* **2011**, *32*, 1760–1775. [CrossRef]
19. Bonin, L.; Vitry, V.; Delaunois, F. Replacement of lead stabilizer in electroless nickel-boron baths: Synthesis and characterization of coatings from bismuth stabilized bath. *Sustain. Mater. Technol.* **2020**, *23*, e00130. [CrossRef]
20. Vijayanand, M.; Elansezhian, R. Influence of surfactants on the properties of electroless nickel boron (thallium and lead-free) coatings. *Proc. Inst. Mech. Eng. Part E J. Process Mech. Eng.* **2018**, *232*, 12–22. [CrossRef]
21. Yin, X.; Hong, L.; Chen, B.H.; Ko, T.M. Modeling the stability of electroless plating bath—Diffusion of nickel colloidal particles from the plating frontier. *J. Colloid Interface Sci.* **2003**, *262*, 89–96. [CrossRef]

22. Abd El-Rehim, S.S.; Shaffei, M.; El-Ibiari, N.; Halem, S.A. Effect of additives on plating rate and bath stability of electroless deposition of nickel-phosphorus-boron on aluminum. *Met. Finish.* **1996**, *94*, 29–33. [CrossRef]

23. Gad, M.R.; El-Magd, A. Additives for electroless nickel alloy coating processes. *Met. Finish.* **2001**, *99*, 77–83. [CrossRef]

24. Mallory, G.O. The electroless nickel plating bath: Effect of variables on the process. In *Electroless Plating: Fundamentals and Applications*; American Electroplaters and Surface Finishers Society: Orlando, FL, USA, 1990; pp. 57–101.

25. Delaunois, F.; Petitjean, J.P.; Lienard, P.; Jacob-Duliere, M. Autocatalytic electroless nickel-boron plating on light alloys. *Surf. Coat. Technol.* **2000**, *124*, 201–209. [CrossRef]

26. Oliver, W.C.; Pharr, G.M. An improved technique for determining hardness and elastic modulus using load and displacement sensing indentation experiments. *J. Mater. Res.* **1992**, *7*, 1564. [CrossRef]

27. Bonin, L.; Vitry, V.; Delaunois, F. Influence of the anionic part of the stabilizer on electroless nickel-boron plating. *Mater. Manuf. Process.* **2018**, *33*, 227–231. [CrossRef]

28. Vitry, V.; Sens, A.; Delaunois, F. Comparison of various electroless nickel coatings on steel: Structure, hardness and abrasion resistance. In *Materials Science Forum*; Trans Tech Publications Ltd.: Zurich, Switzerland, 2014; Volume 783, pp. 1405–1413. [CrossRef]

29. Matik, U. Akımsız Ni-B kaplanmış demir esaslı toz metal kompaktlarin sertlik ve yapisal özelliklerine isil işlemin etkisi. *Gazi Üniversitesi Fen Bilim. Derg. Part C Tasarım ve Teknol.* **2017**, *5*, 223–230.

30. Baskaran, I.; Narayanan, T.S.N.S.; Stephen, A. Effect of accelerators and stabilizers on the formation and characteristics of electroless Ni-P deposits. *Mater. Chem. Phys.* **2006**, *99*, 117–126. [CrossRef]

31. Riddle, Y.W.; Bailer, T.O. Friction and wear reduction via an Ni-B electroless bath coating for metal alloys. *Jom* **2005**, *57*, 40–45. [CrossRef]

32. Vitry, V.; Bonin, L. Increase of boron content in electroless nickel-boron coating by modification of plating conditions. *Surf. Coat. Technol.* **2017**, *311*, 164–171. [CrossRef]

33. Lee, K.H.; Chang, D.; Kwon, S.C. Properties of electrodeposited nanocrystalline Ni-B alloy films. *Electrochim. Acta* **2005**, *50*, 4538–4543. [CrossRef]

34. Arias, S.; Castaño, J.G.; Correa, E.; Echeverría, F.; Gómez, M. Effect of heat treatment on tribological properties of Ni-B coatings on low carbon steel: Wear maps and wear mechanisms. *J. Tribol.* **2019**, *141*, 091601. [CrossRef]

35. Çelik, I.; Karakan, M.; Bülbül, F. Investigation of structural and tribological properties of electroless Ni-B coated pure titanium. *Proc. Inst. Mech. Eng. Part J J. Eng. Tribol.* **2016**, *230*, 57–63. [CrossRef]

36. Balaraju, J.N.; Priyadarshi, A.; Kumar, V.; Manikandanath, N.T.; Kumar, P.P.; Ravisankar, B. Hardness and wear behaviour of electroless Ni–B coatings. *Mater. Sci. Technol.* **2016**, *32*, 1654–1665. [CrossRef]

37. Krishnaveni, K.; Sankara Narayanan, T.S.N.; Seshadri, S.K. Electroless Ni-B coatings: Preparation and evaluation of hardness and wear resistance. *Surf. Coat. Technol.* **2005**, *190*, 115–121. [CrossRef]

38. Vitry, V.; Bonin, L. Effect of temperature on ultrasound-assisted electroless nickel-boron plating. *Ultrason. Sonochem.* **2019**, *56*, 327–336. [CrossRef]

39. Correa, E.; Mejía, J.F.; Castaño, J.G.; Echeverría, F.; Gómez, M.A. Tribological characterization of electroless Ni-B coatings formed on commercial purity magnesium. *J. Tribol.* **2017**, *139*, 1–9. [CrossRef]

40. Hertz, H. *Hertz's Miscellanous Papers*; Macmillan: London, UK, 1896.

41. Zhang, P.; Li, S.X.; Zhang, Z.F. General relationship between strength and hardness. *Mater. Sci. Eng. A* **2011**, *529*, 62–73. [CrossRef]

42. Baskaran, I.; Sankara Narayanan, T.S.N.; Stephen, A. Corrosion resistance of electroless Ni-low B coatings. *Trans. Inst. Met. Finish.* **2009**, *87*, 221–224. [CrossRef]

43. Kanta, A.F.; Vitry, V.; Delaunois, F. Wear and corrosion resistance behaviours of autocatalytic electroless plating. *J. Alloys Compd.* **2009**, *486*, 21–23. [CrossRef]

44. Bonin, L.; Vitry, V.; Delaunois, F. Corrosion behaviour of electroless high boron-mid phosphorous nickel duplex coatings in the as-plated and heat-treated states in NaCl, H_2SO_4, NaOH and Na_2SO_4 media. *Mater. Chem. Phys.* **2018**, *208*, 77–84. [CrossRef]